gels

MDPI

Article

Matured myofibres in bioprinted constructs with *in vivo* vascularisation and innervation

Catherine GY Ngan [1,3,5,6,*], Anita Quigley [2,4,5,6,7], Richard J Williams [6,8], Cathal D O'Connell [6,7], Romane Blanchard [1,3], Mitchell Boyd-Moss [7,8], Tim D Aumann [9], Penny McKelvie [10], Gordon G Wallace [5,11], Peter FM Choong [1,3,5,6], Rob MI Kapsa [2,4,5,6,7,*]

1 Department of Surgery, The University of Melbourne, St Vincent's Hospital, Melbourne, Australia ; cgy.ngan@gmail.com
2 Department of Clinical Neurosciences, St Vincent's Hospital, Melbourne, Australia
3 Department of Orthopaedics, St Vincent's Hospital, Melbourne, Australia
4 Department of Medicine, The University of Melbourne, Melbourne, Australia
5 ARC Centre of Excellence for Electromaterials Science, University of Melbourne, Australia
6 Biofab3D@ACMD, St Vincent's Hospital, Melbourne, Australia
7 School of Engineering, RMIT University, Bundoora, Australia
8 School of Medicine, Deakin University, Waurn Ponds, Australia
9 Florey Institute of Neuroscience and Mental Health, Australia
10 Department of Anatomical Pathology, St Vincent's Hospital, Melbourne, Australia
11 ARC Centre of Excellence for Electromaterials Science, University of Wollongong, Australia

* Correspondence: CGYN cgy.ngan@gmail.com; RMIK rob.kapsa@rmit.edu.au

Abstract: The study of tissue-engineered skeletal muscle has for decades been driven by a clinical need to treat neuromuscular diseases and volumetric muscle loss. The in vitro fabrication of muscle offers the opportunity to test drug and cell-based therapies, to study disease processes, and to perhaps one day serve as a muscle graft for reconstructive surgery. This study developed a biofabrication technique to engineer muscle for research and clinical applications. A bioprinting protocol was established to deliver primary mouse myoblasts in a gelatin methacryloyl (GelMA) bioink, which was implanted in an in vivo chamber in a nude rat model. For the first time, this work demonstrated the phenomenon of myoblast migration through the bioprinted GelMA scaffold, with cells spontaneously forming fibres on the surface of the material. This enabled advanced maturation and facilitated the connection between incoming vessels and nerve axons in vivo without the hindrance of a scaffold material. Immunohistochemistry revealed hallmarks of tissue maturity, with sarcomeric striations and peripherally placed nuclei in organised bundles of muscle fibres. Such engineered muscle autografts could, with further structural development, eventually be used for surgical reconstructive purposes, whilst the methodology presented here specifically has wide applications for in vitro and in vivo neuromuscular function and disease modelling.

Keywords: skeletal muscle, tissue engineering, neuromuscular, bioprinting, GelMA

Citation:

Academic Editor:

Received:
Accepted:
Published:

1. Introduction

Skeletal muscle is a dynamic, vascularised and innervated tissue that supports stature and all voluntary movement in the body. While it has the capacity to regenerate and self-repair from small injuries, volumetric muscle defects and genetic myopathies contribute to a significant healthcare burden [1,2]. The study of these diseases and development

of treatments require faithful models of skeletal muscle physiology and anatomy in order to demonstrate efficacy and safety prior to translation into clinical trials [3,4]. However, the search for muscle models in vitro has been limited by biofabrication techniques that result in poor diffusion of cell nutrients, are not permissive for integration of nerves and vessels, and as a consequence hinder maturation of the engineered tissues [5].

Neogenesis of skeletal muscle in vitro relies on emulation of the in vivo environment, which must simulate the regenerative cell niche to sufficiently direct and sustain the differentiation of muscle progenitors from regenerative myoblasts to functional multinucleated myofibres . While traditional muscle regeneration methods endeavour to recapitulate the stem cell niche in two-dimensional cultures, such techniques do not translate well to the fabrication of larger constructs for clinical applications [5]. Three-dimensional (3D) cultures introduce volume, can better promote cell maturation, and offer more accurate models of cell interaction with other systems such as nerves and vasculature [6-8].

Key to 3D engineering of skeletal muscle is the fabrication of a porous scaffold to allow for the diffusion of nutrients and cell waste, while mimicking the native mechanical and biochemical properties of muscle. Bioprinting, a fabrication technique that involves the extrusion of cell-carrying hydrogel 'bioinks' into multilayered filaments, has the potential to address these conditions. This would require the development of a muscle-specific ink, which would form the scaffold for successful cell culture while possessing the material properties required for printing [9,10]. A candidate for this ink is gelatin methacryloyl (GelMA), one of the few biomaterials that can print free-standing structures without a secondary support material due to its gelation properties at low temperatures [11-13]. Its tuneable mechanical and biochemical properties make it a versatile material for tissue engineering, and early work with immortalised myoblast cell lines has demonstrated cell attachment and high cell viability [14-187].

Following the careful in vitro construction of fabricated muscle, survival in vivo depends on the rapid development of critical neuromuscular connections and neovasculature. Common sites of implantation, such as the subcutaneous space or adjacent to muscle compartments, are poor sources of blood vessels, which would significantly limit the development of muscle and its neural connection [9, 10, 198]. An alternative system is to use a surgically-created arteriovenous loop (AV loop) in a dedicated tissue chamber. This approach creates a vascular pedicle for the tissue that can be harvested wholly for transplantation elsewhere [2019-232]. For skeletal muscle, the further inclusion of a motor nerve along with the AV loop would provide an optimal environment for the innervation and vascularisation of the tissue-engineered construct [24]. The use of an *in vivo* culture chamber isolates the system for interrogation of specific interactions between neurovascular structures and the muscle construct, as well as minimizing any accidental harvest of native muscle.

Much of the existing literature has focused on the mechanical and chemical characterisation of potential scaffold biomaterials, with subsequent examination of myoblasts limited to a perfunctory demonstration of in vitro cell viability and the alignment of myotubes. In contrast, this study investigated GelMA as a bioink specifically for skeletal muscle tissue engineering, with systematic assessment of cytotoxic elements in the bioprinting process to optimise the material for in vitro myogenesis. Finally, the bioprinted muscle structures were implanted in an AV loop chamber, to assess its viability and development in vivo and to interrogate its potential for applications in regenerative medicine.

3. Materials and Methods

GelMA hydrogel synthesis

Gelatin methacryloyl (GelMA) was synthesised and sterilised as previously described [253], with a single batch GelMA (degree of functionalisation, 86%) used for this study. A stock solution of 20% w/v GelMA was made for subsequent dilutions. This was achieved by adding sterile phosphate buffered saline (PBS, Thermo Fisher Scientific)

to a known mass of freeze-dried filter-sterilised GelMA, with the addition of 100U/mL penicillin and 100µg/mL streptomycin (Gibco). The material was dissolved at 37°C on a shaker.

Photocuring

A 2% stock solution of Lithium phenyl-2,4,6-trimethylbenzoylphosphinate (LAP) (Tokyo Chemical Industry) was made with PBS, then filter-sterilised (0.22µm filter). This concentration was used for subsequent dilutions in combination with GelMA. The material was photocured with a 365nm UV source (Omnicure LX400+, Lumen DynamixLDGI), without a focusing lens to allow for a more diffuse light with lower intensity. Light intensities were checked with a UV meter (Omnicure R2000 UV Radiometer) before each experiment.

Rheology

Rheological testing was performed on an Anton Paar Rheometer MCR 302, with a 15mm 1° cone plate geometry and a quartz crystal stage. Temperature-dependent gelation kinetics were investigated with a temperature sweep under oscillation (1% strain and 10 rad/s) by cooling at 1.32°C/min from 37°C to 4°C. Viscosity as a function of uncured GelMA was assessed as a function of shear rate (0-100/s) at 4°C. *In situ* UV curing was performed with the Omnicure LX400+ UV light source, fitted to project through the underside of the quartz crystal stage. Two UV intensities were investigated (15mW/cm² and 40mW/cm²) to determine the time required for the storage modulus to plateau. The UV meter was used to measure the light intensity at the sample position.

Compression testing

Different concentrations of GelMA (increments between 6-12% w/v) were prepared with 0.1% w/v LAP. Triplicate samples for mechanical testing were prepared by casting 80µL of GelMA into moulds 2mm in depth. Samples were incubated at 4°C for 20 minutes prior to crosslinking at 4mW/cm² with UV light (365nm) at room temperature for 400 seconds. Samples at room temperature were similarly prepared as a point of comparison. Samples were removed from the moulds and left overnight in PBS at 37°C. Mechanical testing was performed following the protocol as previously described [264]. A TA Electroforce 5500 mechanical loading device (TA Instruments, New Castle, USA) was fitted with a calibrated 5 lbf load cell. Experiments were conducted at room temperature, and samples kept hydrated with PBS during testing. The contact area of the sample was first measured by microscopy imaging. The compression plate was lowered at 0.01 mm/s until the total displacement was 15% of the original height, which was calculated from the point of inflexion of the load vs time curve. Load and displacement was converted into stress (σ) and strain (ε) data using the sample surface area and height. The compressive modulus was computed using stress data between 10 and 15% strain as follows: $E_c = (\sigma_{15} - \sigma_{10})/(\varepsilon_{15} - \varepsilon_{10})$.

Primary myoblast cell culture

Mouse myoblast cultures were prepared from skeletal muscle removed from the hind limbs of three to four week old C57BL/6 mice as previously described [275]. The muscle tissue was finely minced with scissors in digestion buffer (Ham's F-10 (Gibco), 400 U/mL penicillin, 400 µg/mL streptomycin, 1µg/mL amphotericin B (Gibco) and 2.5mM calcium chloride). 10mg/mL Collagenase D (Roche) and 2.4 U/mL Dispase II (Roche) were added, and the tissue incubated for two hours at 37°C. The muscle slurry was then preplated using plain tissue-culture flasks: twice for 20 minutes, once for 40 minutes, then at 24 hour intervals for the next five days in myoblast growth media (Ham's F-10 (Gibco), 20% foetal bovine serum (Gibco), 2.5ng/mL recombinant human basic fibroblast growth factor (bFGF), 2mM L-glutamine (Gibco), 100U/mL penicillin and 100µg/mL of streptomycin (Gibco)). Myoblasts were maintained in growth media at 37°C under 5% CO_2, and passaged at 80% confluence with dissociation buffer (8.5mM NaCl, 0.5mM KCl, 2.3 mM $NaHCO_3$, 0.8mM $NaH_2PO_4.2H_2O$, 0.56mM Glucose, 0.096mM EDTA, 10ng/mL Phenol red, Trypsin (Life Technologies) at 0.25%) and resuspended in myoblast proliferation media.

Myoblast encapsulation in GelMA

Myoblasts cultured to 70-80% confluency in tissue culture flasks were trypsinised, counted and resuspended in growth media. The cell suspension was combined with GelMA warmed to 37°C, 0.1% LAP, 100U/mL penicillin and 100µg/mL of streptomycin. The volumes of cell suspension and 20% w/v stock GelMA were titrated to form the necessary final concentrations of GelMA. For testing of GelMA for cell viability and differentiation, a concentration of five million cells/mL was used to cast into 96 well plates with a volume of 40µL per well (average thickness of 1mm). Ultra-low attachment wells (for suspension cultures) were used for these experiments. Photocuring was performed with exposure to 4mW/cm^2 UV light (365nm) at room temperature for 400 seconds. After curing, the gels were gently washed with PBS, covered in myoblast growth media and incubated in tissue culture conditions at 37°C and 5% CO_2. For bioprinting, the same process was repeated but with 20 million cells/mL [28]. The bioink was transferred to a sterilised printing cartridge (CELLINK), and incubated at 4°C for 20 minutes.

Bioprinting

Bioprinting was performed using a commercial printer (INKREDIBLE+, CELLINK), conducted at room temperature. 27G cone-shaped nozzles (Nordson EFD) were used for printing. A parametric study on fibre diameter as a function of printing speed was firstly performed on 8% w/v GelMA that had been cooled in the cartridge to 4°C for 20 minutes prior to printing. Square crosshatch grids (two layers of 10mm fibres laid down at 0° and 90°, spaced 2.5mm apart, finished with an outer 11mm x 11mm border) were printed in six-well tissue culture plates at speeds between 500 to 1250 mm/min. Plates were kept at 4°C prior to printing. Printing pressures were kept at an average of 60kPa, which was the pressure required to initiate and maintain a steady flow of ink. Fibres were crosslinked and left in PBS overnight at 37°C. Fibre diameters were measured in three areas in triplicate samples at each speed. The bioink formulation (with cells) was then printed at 1000mm/min. After printing, constructs were immediately photocured with exposure to 4mW/cm^2 UV light (365nm) at room temperature for 400 seconds. After curing, the gels were gently washed with PBS, covered in myoblast growth media and incubated in tissue culture conditions at 37°C and 5% CO_2.

Myoblast differentiation

After photo-crosslinking, GelMA constructs (cast or printed) were kept in myoblast growth media at 37°C under 5% CO_2. After 24 hours, the media was changed to myoblast differentiation media (DMEM (Lonza), 2% horse serum (Gibco), 2mM L-glutamine (Gibco), 100U/mL penicillin and 100µg/mL streptomycin (Gibco)). Cells were maintained with daily half-media changes for the duration of culture. After 48 hours, printed constructs were eased off the bottom of the tissue culture plate with a pipette tip, if they were not already afloat in the media.

Myoblast cell viability

Myoblast density in 2D cultures was 10 000 cells/well in a 96-well plate, with a change from growth to differentiation media the day after seeding. Myoblast density for 3D cultures was five million cells/mL of GelMA, again with a change to differentiation media the day after seeding. Two cytotoxicity screening tests were performed: comparing different concentrations of LAP with adjusted UV crosslinking times, and incubation of cultures at 4°C for 20 minutes before transfer to tissue culture conditions. Three time-points at day 0 (24 hours after seeding), 7 and 14 of differentiation were assessed. Cell viability was measured by removing culture medium and incubating the cells with 1µM Calcein-AM (green fluorescence) and 2µM ethidium homodimer (red fluorescence) in sterile PBS. Cells were incubated for 30 minutes at 37°C, and then observed under a fluorescence microscope (EVOS XL Core cell imaging system, Thermo Fisher Scientific). Cell cytotoxicity for different concentrations of LAP was also assessed with Cell Titre-Blue tests (Promega) for the day 0 timepoint, as per the manufacturer's protocols and in triplicate, with the fluorescent signal acquired with a CLARIOstar microplate reader (BMG LABTECH). Cell viability of myoblasts after bioprinting was also investigated at three timepoints with the same techniques as above, at days 0 (24 hours after printing), 7 and 14 of

differentiation. The number of dead cells was counted with Image J software (National Institute of Health) in three fields at 10x magnification. The final unit for quantifying cell death was number of dead cells per 0.1mm^2 of fibre area.

Fluorescent staining and imaging

GelMA-myoblast constructs were fixed with 10% formalin for 30 minutes, then blocked and permeabilised for an hour with 10% normal donkey serum made up with PBS-0.1% TritonX-100. Immunofluorescent staining was performed for sarcomeric myosin (mouse anti-MF20, Developmental Studies Hybridoma Bank). Cells were incubated in the primary antibody (1:400) overnight at 4°C. Cells were then incubated with the secondary antibody Alexa Fluor 594 conjugated donkey anti-mouse IgG (1:2000, Molecular Probes) and Alexa Fluor 488 Phalloidin (1:100, Thermo Fisher Scientific) for 60 minutes at 37°C. Nuclei were stained with 1μg/mL of 4',6-diamidino-2-phenylindole (DAPI, Sigma-Aldrich) for 15 minutes at room temperature. Samples were washed in PBS and imaged with an inverted fluorescence microscope (Olympus IX70). 3D rendered z-stack images were taken with confocal microscopy. 0.5μm red fluorescent beads at a concentration of 25μL/mL were added to the bioink (aqueous suspension of carboxylate-modified polystyrene latex beads, Sigma-Aldrich). After printing, the cells were then stained with Alexa Fluor 488 Phalloidin as described above. Confocal imaging was performed with a NikonA1Plus confocal microscope using a Nikon Plan Fluor 20x DIC L N1 N.A. 0.75 objective lens, with images processed using NIS-Elements software (Nikon).

RT-qPCR

Real-time quantitative reverse transcription polymerase chain reaction (RT-qPCR) was performed on a QuantStudio 6 Flex Real-Time PCR system. Total RNA from bioprinted constructs and 2D control myoblast cultures (grown on tissue culture plastic) were harvested at Days 0, 3, 7 and 14 of differentiation with TRIzol Reagent (Ambion, Thermo Fisher Scientific). The bioprinted constructs were broken down by snap-freezing in liquid nitrogen and then ground with a mortar and pestle. The RNA was purified using the RNeasy Microkit (Qiagen) and assessed with nanodrop quantification (CLARIOStar Monochromator Microplate Reader, BMG Labtech). Reverse transcription was performed using Omniscript RT kit (Qiagen) for 450ng of RNA. Expression of MYOG, MYF6, SIX4, MYH1 and MYH8 was evaluated with SYBR Green Real-Time PCR Master Mix assays (Thermo Fisher Scientific). The 2^ΔΔCT comparative method was used to evaluate relative changes in gene expression, with GAPDH as the housekeeping gene [29~~6~~]. Statistical analysis was performed with unpaired t-tests on three technical replicates. The relevant primers are listed in Table 1.

Table 1. Primer sequences

Name	Forward primer	Reverse primer
Myogenin (MYOG)	5′-GCGCCATCCAGTACATT-GAGC-3′	5′-ACGATGGACGTAAGGGAG-TGC-3′
Myogenic factor 6 (MYF6)	5′CGGAGTGCCATCAGC-TACATTG-3′	5′-TCCACGTTT-GCTCCTCCTTCC-3′
Homeobox protein SIX4 (SIX4)	5′-TTC AAG GAG AAG TCG CGC AAC-3′	5′-ACT GGG GTT GCC ATC CGA TTC-3′
Myosin heavy chain 1 (MYH1)	5′-GGCACTGTGGAC-TACAACATCG-3′	5′-TTT CTT TCC ACC ACC GCC ACC-3′
Myosin heavy chain 8 (MYH8)	5′-CTAC-CAAAGGCAAGGCCGAG-3′	5′-ATCTGCTTCAGCACTAGCG-TATG-3′
Glyceraldehyde 3-phosphate dehydrogenase (GAPDH)	5′-ACAACTTTGGCATTGTG-GAAGGG-3′	5′-TACTTGG-CAGGTTTCTCCAGGC-3′

Scanning Electron Microscopy (SEM) and Scanning Electron Cryomicroscopy (cryoSEM)

Samples were prepared for SEM as follows: bioprinted constructs were fixed in 2.5% paraformaldehyde for 30 min at 37°C, then rinsed three times with sodium cacodylate buffer for five minutes each. Samples were passed through successive dehydration steps in ethanol (50%, 70%, 90% and 95% ethanol for 10 mins, and 100% ethanol for 15 mins). The samples were then dried by soaking in a hexamethyldisilazane (HMDS) solution overnight and attached on the SEM stubs. Finally, the samples were sputter coated with 10 nm gold. Images were observed using FEI Verios 460L FEGSEM under high vacuum conditions. Samples were prepared for cryoSEM as follows: bioprinted constructs were positioned onto a cryoSEM sample holder and plunged into liquid nitrogen (LN_2) slush to snap freeze samples and avoid ice crystal formation. Frozen samples were placed in a sample preparation chamber maintained at -180°C under high vacuum conditions. Next, samples were sublimated at -90°C for two minutes. Finally, samples were gold sputter coated for 120 seconds. Images were observed using FEI Quantra 200 in cryoSEM mode, at -180°C under high vacuum. Images were taken at 15kV.

Calcium imaging

Intracellular calcium transients were assessed by loading bioprinted grids with 5µm Fluo-4 AM dye in extracellular recording solution (145mM NaCl, 5mM KCl, 2.6mM $CaCl_2$, 1mM $MgCl_2$, 10mM Na-HEPES, 5.6mM D-glucose at pH 7.4) [30~~27~~]. After 20 minutes of incubation at 37°C, the dye was removed and the cells incubated for another 20 minutes in fresh extracellular solution. Activity was observed under a fluorescent microscope (Eclipse FN1, Nikon) and recorded with Visiview imaging software (Visitron Systems GmbH). Fluorescence images were recorded with a iXon Ultra camera at 6.67Hz for 90 seconds (Oxford Instruments). Videos were analysed with ImageJ software (National Institute of Health). Calcium transients were expressed as $\Delta F/F$ ($(F_{max}-F_{rest})/F_{rest}$).

***In vivo* study**

A computer-aided design (CAD) file was created using Tinkercad (Autodesk Inc.) for the 3D printing of chambers to house the bioprinted muscle and AV loop. The chamber design was based on similar devices previously described [2~~2~~1,31~~28~~], with modifications to accommodate for the bioprinted muscle. Structures were printed in High Quality,

glossy-finish settings with MED610 (Stratasys) on an Objet30 3D printer (Stratasys). The chambers were cleaned and sterilised following a previously described protocol [32~~29~~]. Chambers were soaked in sterile PBS overnight before use. Bioprinted grids of muscle were differentiated *in vitro* for one week, prior to transfer into chambers for *in vivo* implantation. Two chambers were prepared with bioprinted muscle, while two chambers were prepared with GelMA-only (acellular) grids to serve as controls. This study was approved by the St Vincent's Hospital (Melbourne) Animal Ethics Committee (AEC Ref No: 010/18-r3) and conducted at St Vincent's Experimental and Medical Surgical Unit (EMSU) in accordance with institutional ethics guidelines. Male CBH/rnu/rnu (nude rats) (ARC, Perth, Western Australia) were used for this experiment. Animals weighed a minimum of 250g (15-16 weeks old). All animals were anaesthetised with oxygen/isoflurane inhalation (2L O_2/2% isoflurane) and received a subcutaneous dose of Carprofen (5mg/kg) pre-operatively. Prior to implantation, the differentiated bioprinted muscle grids were transferred onto the base of the chamber in a class II biosafety cabinet, before being taken to the sterile operating field. Samples were kept hydrated with media up until implantation. Loop surgeries were performed by animal technicians expert at microsurgery at EMSU as previously described [22~~1~~,23~~2~~]. In brief, an AV loop was constructed in the left groin by firstly taking a vein graft from the right femoral vein. The vein was interposed between proximal stumps of the right femoral artery and vein with end to end anastomosis using 10-0 monofilament nylon sutures. This loop was placed in the chamber along with the transected femoral nerve. The chamber was secured to surrounding tissue with 6-0 prolene sutures through holes in the outer perimeter of the base. The chamber was kept open during the whole procedure to observe patency (pulsation) of the AV loop. The lid was clipped on top of the chamber, and the skin was closed in layers with 4.0 silk sutures. Animals were monitored post-operatively until they were recovered from anaesthesia and able to move around the cage. Post-op care and monitoring was carried out as per institutional guidelines. All animals remained well throughout the two-week period, with good wound healing and general health. After two weeks, the animals were anaesthetised and the chambers wholly retrieved by resecting the neurovascular bundle at the chamber entrance. The contents of the chamber were submerged in 10% formalin for 24 hours, sectioned at 3mm intervals, and processed into paraffin wax.

Histology

Paraffin blocks were cut at 5μm sections for haematoxylin and eosin (H&E) staining and immunohistochemistry. Immunofluorescent staining was performed for desmin (rabbit anti-desmin, 1:100, Abcam) and beta-III tubulin (mouse anti-B3T, 1:200, Covance). Sections were dewaxed in three changes of 100% xylene, rehydrated in ethanol series (100%, 80%, 60%, 30% and water for five minutes each) and underwent antigen retrieval in citrate buffer (10mM, pH 6). Sections were washed and blocked in 10% goat serum for one hour at room temperature. Primary antibodies were added to the slides and left overnight at 4°C. Cells were incubated in the secondary antibodies Alexa Fluor 594 conjugated goat anti-mouse IgG (1:2000, Molecular Probes) and Alexa Fluor 488 conjugated goat anti-rabbit IgG (1:2000, Molecular Probes) for 60 minutes at 37°C. Slides were washed in PBS before mounting with Fluoroshield with DAPI (Abcam). Slides were imaged with an inverted fluorescence microscope (Olympus IX70). Confocal imaging was performed with a NikonA1Plus confocal microscope using a Nikon Plan Fluor 20x DIC L N1 N.A. 0.75 objective lens, with images processed using NIS-Elements software (Nikon). All samples were sectioned and stained at three different levels.

Statistical analysis

Data is presented as mean ± standard deviation (SD). GraphPad Prism 5 software (San Diego, California, USA) was used for statistical analysis. PCR data was analysed by performing unpaired t-tests, with statistical significance defined as $p < 0.05$.

3. Results

~~**Printing myoblasts encapsulated in a GelMA bioink**~~**Optimising myoblast culture in cast GelMA samples**

Myoblasts were encapsulated and photo-crosslinked in GelMA that had undergone rheological characterisation and was optimised for cell viability, thus defining LAP concentration, temperature and photo-curing time (Appendix Figures A1 and A2). A similar degree of cell fusion and myotube formation was observed in all the GelMA concentrations, despite the compressive moduli ranging from 40 to 260 kPa (Figure 1). 3D-rendered confocal micrographs demonstrated cell migration through GelMA over two weeks of culture. By day 14, most cells had migrated to the material boundary to form an extensive layer of myotubes. This experiment was performed in low-adhesion tissue culture plates to eliminate the possibility of cells growing on the plastic below the material. 8% w/v GelMA was used for subsequent experiments, given that there was no morphological difference between GelMA concentrations.

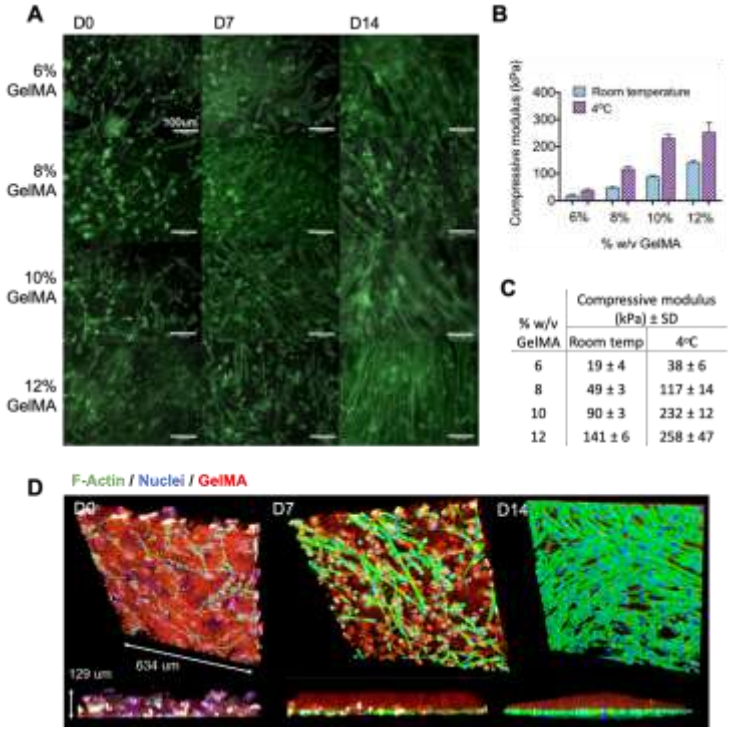

Figure 1. Characterisation of GelMA concentrations. A) Myoblasts were encapsulated in 6, 8, 10 and 12% w/v GelMA and differentiated over 14 days to establish the optimal formulation for myo-regenerative cells. Samples were fixed and stained for F-actin at days 0, 7 and 14, revealing similar myotube morphology in all concentrations. B,C) Compressive moduli of the different percentages of GelMA samples at room temperature and at 4oC, measured without cells. Error bars represent standard deviation. D) 3D rendered confocal images of myoblasts encapsulated in GelMA, with images taken at days 0, 7 and 14 of differentiation. 8% w/v GelMA was chosen as a representative sample. Myofibres were stained for F-actin (green) and ~~DAPI~~ DNA (blue), and GelMA was demarcated with red fluorescent latex beads. These images demonstrate the migration of myoblasts to the boundary of the material, where they subsequently differentiated into multinuclear myotubes.

Printing myoblasts encapsulated in a GelMA bioink

Printing parameters were defined to produce the finest fibres without thread breakage, with an average fibre diameter of 360μm (Figure 2). Having determined the optimal printing speed, cCell-laden GelMA (20 million cells/mL in 8% GelMA/0.1% LAP) was printed and photocured in a crosshatch pattern. Live/dead cell stains of the bioprinted fibres demonstrated high cell viability both immediately after printing and over two weeks of in vitro differentiation (Figure 3). Cells were again observed to migrate to the perimeters of the printed fibres, where they fused into myotubes on the GelMA surface. This was consistent with myoblast behaviour in cast GelMA samples, with the added observation that myoblasts could migrate out in all directions in the thinner bioprinted constructs. Imaging with cryoSEM further demonstrated an absence of microgrooves on the material surface that might have influenced the direction of myofibre growth. SEM permitted better preservation of cells on the material, and these images demonstrated multilayered myotubes growing on the printed GelMA.

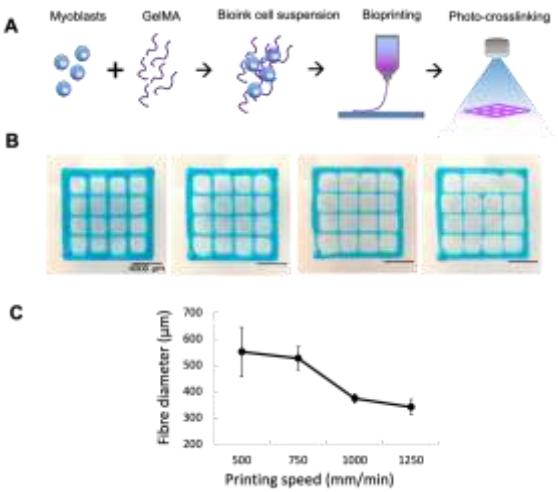

Figure 2. Parametric study of fibre diameters. Constructs were printed with the smallest available CELLINK conical nozzle (27G) at the minimum pressure required to initiate and maintain bioink flow (60kPa). Blue food dye was used for the purpose of imaging. A) Schematic of printing process. B) Printing speeds were compared between 500, 750, 1000 and 1250 mm/min (left to right). 1000 mm/min produced the finest fibres without thread break-up. C) Fibres were soaked in PBS overnight at 37oC before diameters were measured. Error bars represent standard deviation.

Formatted: Font: Bold, Complex Script Font: Bold

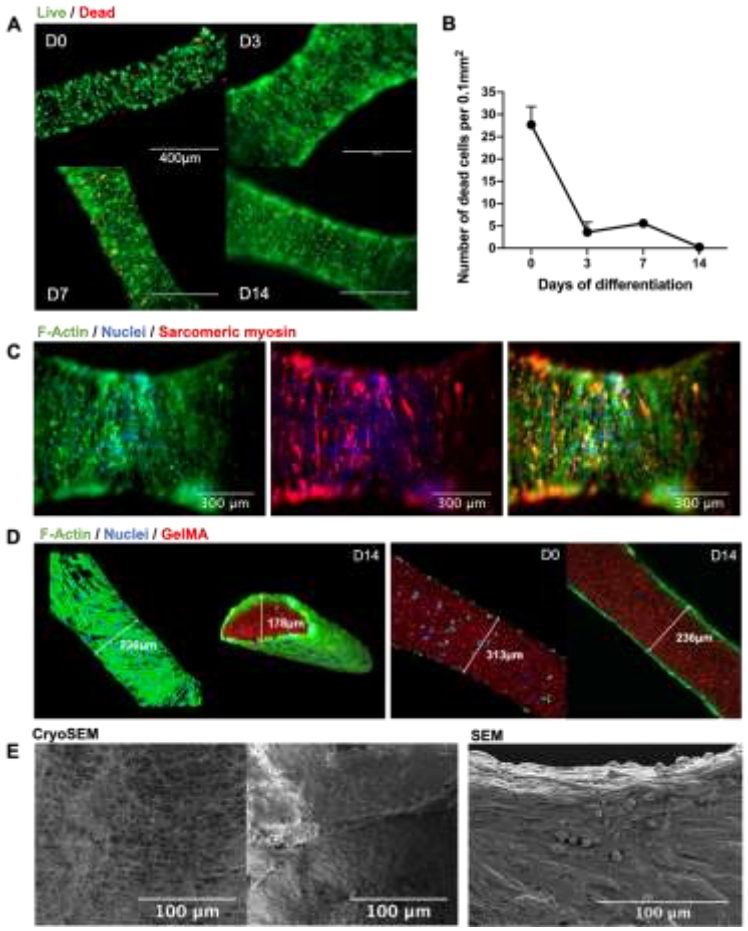

Figure 3. Characterising myoblast behaviour in bioprinted fibres. A) Live (green) / dead (red) cell stains were performed at days 0, 3, 7 and 14 of differentiation after bioprinting. Given the nature of myoblast fusion, live cells were not individually counted, although qualitatively the live stain revealed dense myofibre formation. B) Cell death was reported as a cell count per 0.1mm2 of printed fibre. There was a peak in cell death at day 0, as would be expected due to shear stress during extrusion, followed by a rapid recovery from day 3 through to day 14. Error bars represent standard deviation. C) Cells were stained for F-actin (green), sarcomeric myosin (red) and ~~DAPI~~ DNA (blue). The emergence of myosin-positive fibres is a marker of maturing contractile mechanisms within the myofibre. D) Confocal imaging of cells demonstrated migration from within the GelMA to the boundary of the material, where they fused into multinucleated myotubes on the material surface. E) cryoSEM of bioprinted GelMA showed the nature of myofibre adherence without surface microgrooving or patterning that might have influenced the direction of cell growth. SEM demonstrated a dense multilayered myotube culture on the printed GelMA fibres.

Gene expression analysis of bioprinted muscle

Five gene markers of myogenic maturation were analysed: MYOG, MYF6, SIX4, MYH1 and MYH8. GAPDH was used as the housekeeping gene. MYOG and MYF6 represent two of the four key myogenic regulatory factors that control cell fusion and terminal differentiation, while SIX4 is one of the earliest regulators of myogenic lineage specification [30]. MYH1 and MYH8 encode for the key contractile protein myosin, which exists in several isoforms during development [41].

This analysis of myogenic markers revealed statistically significant differences in gene expression between the 2D control and bioprinted fibres, demonstrating an overall more mature phenotype in the bioprinted fibres (Figure 4). The joint upregulation of MYF6 and downregulation of MYOG is consistent with advanced differentiation. MYOG is known to be expressed prior to terminal differentiation and MYF6 is expressed after myoblast fusion and its presence furthermore down-regulates MYOG [52]. SIX4 was significantly downregulated in the bioprinted fibres, as expected in more differentiated myofibres [63]. Both myosin isoforms were greatly upregulated at day 7 in bioprinted fibres, with an overall trend of more accelerated myosin protein development when compared to the gradual increase in the 2D controls. The subsequent fall in gene expression at day 14 may represent a plateau in myofibre maturation for the bioprinted fibres under these conditions, while the 2D cultures did not reach the same level of myosin gene expression over two weeks.

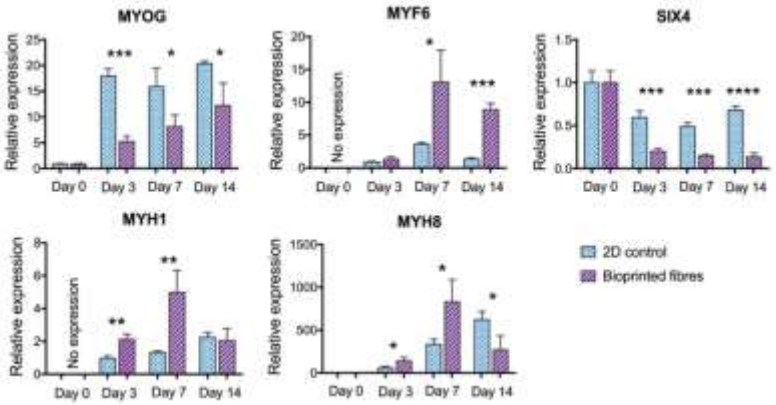

Figure 4. Gene expression demonstrated more advanced myogenesis in bioprinted fibres. The graphs represent the fold changes calculated with the 2^ΔΔCT method. There was a steady-state expression of MYOG in the 2D cultures after day 3, with significantly lower expression in the bioprinted samples at days 3 (p=0.0002), day 7 (p = 0.0295) and day 14 (p = 0.0286). The increase in MYOG in bioprinted samples across timepoints was not statistically significant. MYF6 was undetectable at day 0, but over three-fold higher than the 2D control on day 7 (p = 0.0258) and day 14 (p = 0.0001). SIX4 was significantly downregulated in the bioprinted fibres compared to 2D controls at day 3 (p = 0.0008), day 7 (p = 0.0001) and day 14 (p < 0.0001). Upregulation of MYH8 was significantly greater in bioprinted fibres at day 3 (p = 0.0165), day 7 (p = 0.0292) and day 14 (p = 0.0279). Upregulation of MYH1 was significantly greater in the bioprinted fibres at day 3 (p = 0.0031) and day 7 (p = 0.0084). All asterisks refer to statistically significant differences between 2D control and bioprinted fibres at the same timepoint (*p<0.05, **p<0.01, ***p<0.001, ****p<0.0001). Error bars represent standard deviation.

Functional analysis of bioprinted muscle

Differentiating myoblasts show spontaneous calcium transients due to immature mechanisms that allow flux from intracellular calcium stores and, later on, an influx of extracellular calcium through the immature expression of T-type calcium channels that allow a voltage drift towards the depolarisation threshold [374-396]. The latter mechanism can trigger regular pacemaker activity reminiscent of cardiac myocytes, which is a known feature of developing myofibres before they mature and reach electrical independence [396].

As such, calcium imaging was used to characterise functionality in developing myotubes at days 3, 7 and 14 of differentiation (Figure 5). The amplitude of signal recordings was not quantitatively assessed due to the 3D nature of the culture which influences signal intensity, but the frequency and pattern of activity were recorded. Widespread patterns of calcium flux were observed by day 7, reflective of varying stages of maturation of myofibres at this timepoint. By day 14, sustained regular 'pacemaker-like' activity was observed in the developing myofibres. Fewer active cells were recorded, perhaps due to maturing membrane channels less susceptible to calcium flux.

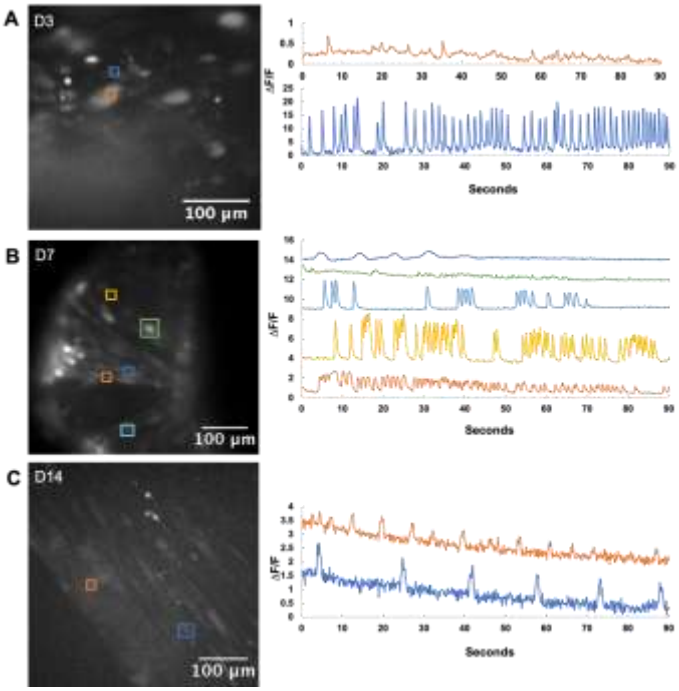

Figure 5. Calcium imaging of bioprinted fibres. Active cells are marked out in the micrographs on the left, with the calcium trace in the corresponding colour on the right. A) Day 3 bioprinted fibres showed minimal activity, with rapid firing occasionally observed from single myoblasts. B) Day 7 bioprinted fibres showed a variety of calcium activity, which is commonly observed during myoblast differentiation. C) By Day 14, active cells had pacemaker activity, characterised by a slower, regular spiking pattern. This is thought to represent a maturation of calcium handling proteins that can respond to depolarisation as well as replenish intracellular stores in time for the next action potential.

Implantation of bioprinted skeletal muscle fibres in vivo

After one week of in vitro differentiation, the bioprinted muscle constructs were housed in 3D-printed chambers supplied with a surgically-formed AV loop and transected femoral nerve in the nude rat model (Figure 6). The chamber was implanted and secured in a subcutaneous pocket in the groin for a further two weeks, after which the contents were retrieved for fixing and staining. Native muscle was not incised during this procedure.

Chamber specimens were sectioned and stained for the muscle-specific protein desmin and the neuronal microtubule beta-III tubulin (Figure 7). Triads of muscle, neovasculature and neuronal sprouting were observed. Regenerating multinucleated myofibres were identified by their centrally located nuclei, and early evidence of innervation was seen in muscle bundles interspersed with B3T-positive structures. Mature muscle morphology was also observed, characterised by sarcomeric striations and peripherally placed nuclei in organised bundles of parallel fibres. The new muscle tissue was largely independent of the original GelMA scaffold, and there was no integration of vasculature or nerves into the GelMA scaffold. Significant neural ingrowth was present in this bundle of mature muscle.

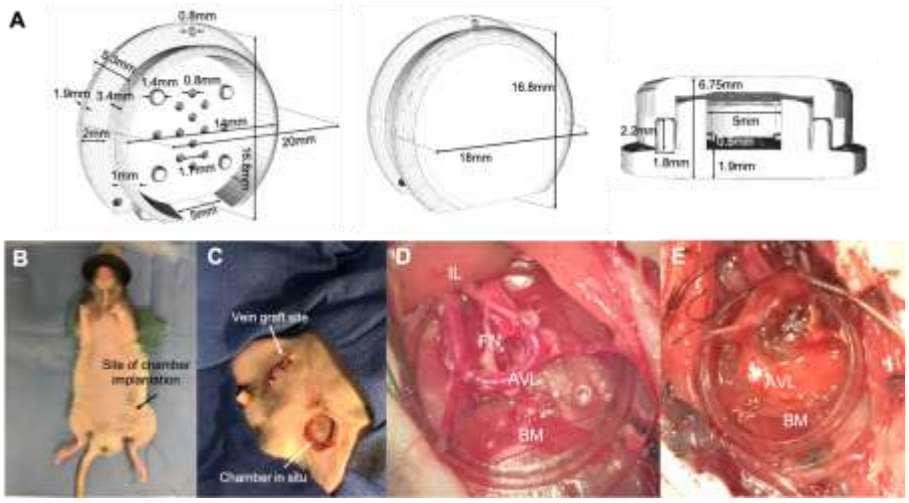

Figure 6. Bioprinted constructs were implanted in vivo for two weeks in an isolated chamber that housed an AV loop and transected femoral nerve. A) The 3D-printed chambers comprised of a base on which the bioprinted grid was positioned, along with a lid that held the contents in place. An opening in the chamber wall allowed for entry and exit of the neurovascular bundle. Perforations in the base allowed for flow of cell media while in tissue culture conditions. B-C) Chambers were positioned in a subcutaneous pocket in the left groin of the rat. Vein grafts were harvested from the right femoral vein to create the AV loop. D) The AV loop and transected femoral nerve was placed on top of the bioprinted muscle grid. BM = bioprinted muscle, AVL = arteriovenous loop, FN = femoral nerve, IL = ilioinguinal ligament. E) Muscle construct 2 weeks after *in vivo* implantation.–

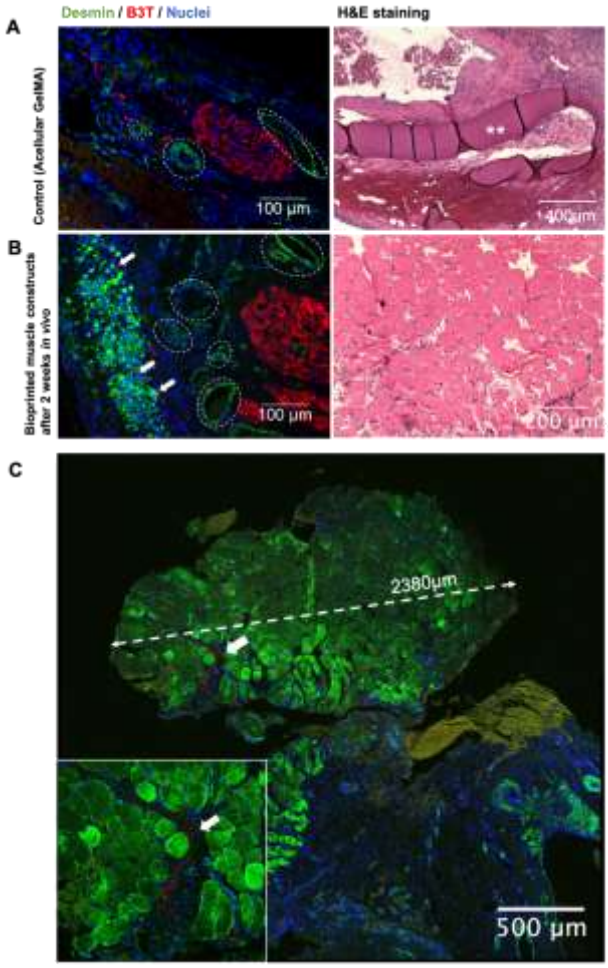

Figure 7. Immunostaining was performed on tissues harvested from the AV loop chambers after two weeks in vivo. Sections were stained for desmin (green), B3T (red) and ~~DAPI~~ DNA (blue). Examples of angiogenesis are marked with dotted lines. Arrows point to neuronal outgrowth. Asterisks label GelMA. ~~(Top~~A) After two weeks of implantation, sections from the GelMA-only controls demonstrated angiogenesis and neuronal sprouting without muscle formation. Blood vessels were identified as ringed desmin-positive structures, due to the smooth muscle encircling the vascular wall. Neuronal outgrowth was observed as clusters of B3T-positive cells. H&E staining revealed the inert characteristics of GelMA, which after two weeks showed no muscular, neural or vascular growth within the material. B) In contrast, tissue from chambers that housed bioprinted grids demonstrated muscle regeneration and maturation. Axonal outgrowth and angiogenesis was present throughout the developing muscle fibres. ~~– H&E staining revealed the inert characteristics of GelMA, which after two weeks showed no muscular, neural or vascular growth within the material. – C(Bottom~~) Confocal micrograph of a 2.38mm bundle of mature skeletal muscle from one of the chambers that housed bioprinted muscle. Inset is the magnified image of neuronal growth within this muscle bundle.

4. Discussion

This study presents a simple, single-material bioprinting technique to engineer functional skeletal muscle fibres capable of advanced maturation for in vivo engineered muscle modelling. Through the systematic evaluation and optimisation of GelMA as a bioink for myoblast cultures, new observations were made regarding cell maturation and migration in this biomaterial. Advanced myofibre development was observed by both molecular and functional analysis. After only two weeks of implantation in vivo, the engineered tissue was capable of vascular and neural integration. These results present a promising approach for rapid 3D fabrication of functional skeletal muscle constructs, with opportunities arising for both lab-based personalised neuromuscular tissue modelling and ultimately, even for clinical applications.

In the process of optimising the material for myoblast cultures, a key outcome was to recognise and subsequently capitalise on the phenomenon of cell migration. 3D-rendered confocal imaging revealed relocation of myoblasts to the boundary of the material in both cast and bioprinted samples. One explanation for this could be the presence of a nutrient diffusion gradient within the hydrogel matrix, as previously described by Wang et al [40~~37~~]. Nonetheless, despite the myoblasts' rather resourcefully transforming a 3D culture system into essentially a pseudo-2D one, this phenomenon was not at all a limitation in the differentiation process. Indeed, it underpins a further observation that a range of GelMA concentrations with consequently differing substrate stiffnesses equally supported myoblast differentiation. While the optimal stiffness for C2C12 myofibres has been reported to be ~12kPa, it is known that actomyosin striation will occur on a second myofibre layer grown on top of a bottom myofibre layer, despite a large range of underlying substrate moduli [41~~38~~,42~~39~~]. Our results add to this literature by demonstrating that myoblasts can further survive encapsulation in a wide range of GelMA concentrations/stiffnesses, after which the cells migrate to form a dense multilayered culture on the surface as seen on SEM imaging. Myofibres were thus able to striate over a wide range of substrate stiffnesses due to the overlay of cells that permitted more advanced differentiation. This ability of myoblasts to compensate for the underlying modulus is an advantage for biofabrication techniques using GelMA, given that stiffer materials are generally easier to handle and have better shape fidelity when printed.

Another critical advantage of myoblast migration is that the final superficial position of the cells obviates the existing conundrum of NMJ formation with engineered muscle. Nerve and muscle have vastly different biological characteristics that are often at odds when choosing a suitable scaffold material. In particular, neural tissues prefer much softer substrates (less than 1kPa), which is generally incompatible with any material optimal to muscle [43~~0~~,44~~1~~]. Thus, the suitability of GelMA for skeletal muscle engineering may be aided by myoblast migration to the surface, which appropriately supports innervation and even vascularisation. It should be noted that the fabrication of fibres with superficial cell growth is not readily achieved with the traditional approach of seeding cells on top of a pre-made scaffold, which is often hindered by poor cell migration through the matrix. Bioprinting allows for specific placement of cells throughout the entire scaffold geometry, and in future could incorporate fibres specific for housing regenerative muscle progenitors and delivering growth factors.

Both molecular and functional analysis demonstrated superior myotube maturation in bioprinted GelMA constructs when compared to 2D controls. Gene analysis supported advanced differentiation with an inverse relationship between the expression of two myogenic regulatory factors MYOG and MYF6, the downregulation of the early myogenic regulator SIX4, and the rapid upregulation of MYH1 and MYH8 that encode the critical contractile protein myosin. This was further reinforced with calcium imaging, which showed a progression towards organised rhythmic calcium transients over two

weeks of in vitro differentiation. This is known to represent maturity of intracellular calcium handling proteins that can respond to and recover from spontaneous membrane depolarisation.

The bioprinted structures were then housed in chambers supplied by a surgically-formed arterio-venous (AV) loop and transected femoral nerve. This proof-of-concept study was designed to assess the feasibility of creating vascularised grafts of muscle from bioprinted structures, and whether neural outgrowth would occur in the presence of GelMA. Containment of these elements in a subcutaneous chamber enabled "in vivo" analysis of their interaction without confounding or synergistic effects from native muscle. GelMA-only controls demonstrated that the chamber supported angiogenesis and neural sprouting in the presence of the material, although without any muscle formation. Immunohistochemical staining of the AV chambers after two weeks in vivo revealed bundles of regenerating and also mature myofibres (striated and peripherally-nucleated), which were integrated with neural outgrowth and neovasculature within the myoblast-containing chambers (but not in the non myoblast-containing chambers).

Another key aspect of this experiment was the role of GelMA in vivo. GelMA transitioned from being a necessary scaffold for the initial differentiation and organisation of myoblasts in vitro, to a temporary support structure for in vivo myofiber differentiation and maturation. The material appeared biologically inert, surrounded by new muscle, vessels and nerves. GelMA is known to degrade in vivo, giving rise to the possibility that with more time, the degradation of GelMA may yield fully tissue engineered muscle [45~~2~~,46~~3~~] within the AV loop system used here. Furthermore, the very rapid differentiation and consequential early structural independence of the developing muscle tissue frees it from being constrained by the degradation rate of GelMA or orientation cues presented by its structural configuration.

5. Conclusion

Effective engineering of skeletal muscle requires a scaffold material that can deliver high cell viability, support myotube maturation and acquisition of functionality, and be permissive to innervation and vascularisation. This work demonstrates myoblast migration through GelMA as a single-material bioink, enabling advanced maturation and facilitating neural and vascular ingrowth. These findings provide a potential means to expedite therapeutic discovery for neuromuscular disorders by modelling fully matured, vascularised and innervated muscle tissue in a small animal model, as well as laying a potential foundation for fabrication of innervated and vascularised muscle grafts. In future works, the application of induced pluripotent stem cells (iPSC) to generate muscle tissue constructs in the AV loop system offers the possibility of personalised treatment options for neuromuscular disease and volumetric muscle loss.

Author Contributions: CGYN designed and performed the experiments and data analyses, wrote the manuscript and prepared the figures. AQ provided intellectual input and technical support with regards to cell analysis and imaging, and edited the manuscript. CDO and RB provided intellectual input and technical support with regards to material analysis, and edited the manuscript. MBM and RJW performed image acquisition with cryoSEM and SEM, and edited the manuscript. TDA provided intellectual input and technical support with regards to the in vivo study. PM provided technical support with regards to histological analysis. GGW, PFMC and RMIK edited and approved the manuscript.

Funding: The work reported was supported by the Aikenhead Centre of Medical Discovery Research Endowment Fund, Australian Research Council and MTPConnect. CN was supported by a NHMRC Postgraduate scholarship (App 1133271). PC is supported by a NHMRC Practitioner Fellowship (App 1154203). Funding from the Australian Research Council Centre of Excellence Scheme (Project Number CE 140100012) is gratefully acknowledged. The authors would also like to thank the Australian National Fabrication Facility (ANFF) – Materials node for access to services and equipment.

593

594

Conflicts of Interest: The authors declare no conflict of interest.

595

596

Appendix

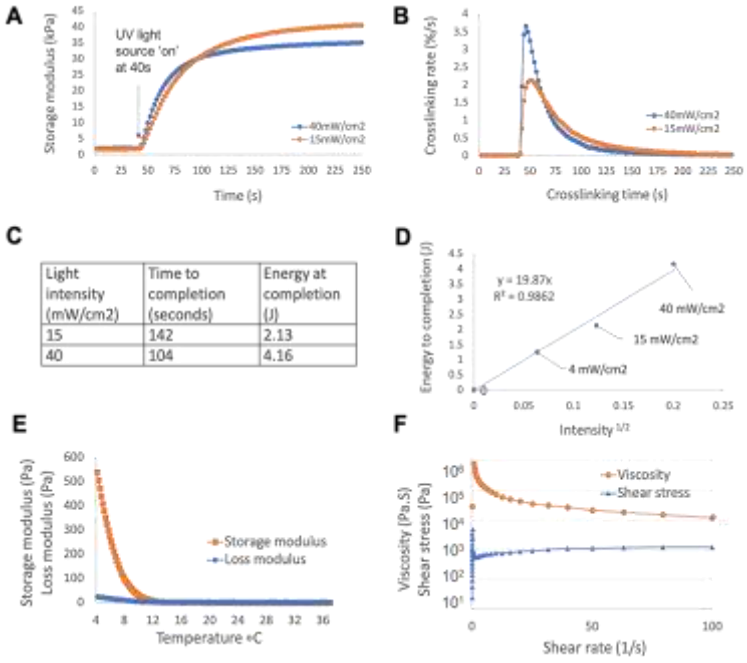

Light intensity (mW/cm2)	Time to completion (seconds)	Energy at completion (J)
15	142	2.13
40	104	4.16

Figure A1. Rheology data for 8% w/v GelMA/0.1% w/v LAP, performed at 4oC unless otherwise specified. A) To calculate crosslinking times of GelMA at 4mW/cm2, the material was more rapidly crosslinked at 40mW/cm2 and 15mW/cm2 with the purpose of extrapolating the data to 4mW/cm2. This was done to minimise the effect of condensation between the material and stage (a consequence of using a quartz plate to allow for in situ UV curing). B) The relative reaction rates for these intensities was defined as the change in storage modulus per second as a percentage of the final modulus after 210 seconds of curing time, a timepoint chosen to approximate completion as it occurs well within the range of the graph approaching plateau. Energy to completion was defined as a relative reaction rate of <0.1%/s, which occurred at 142 seconds at 15mW/cm2, and 104 seconds at 40mW/cm2. C) The energy to crosslink the material could then be estimated by multiplying time (t) by intensity (I): $E = tI$. D) Known relationships between light intensity and crosslinking rate were used to extrapolate this data: $E = k_E\sqrt{\frac{I}{c}}$ where E is the total energy, k_E is the proportionality coefficient, I is the intensity of light and c is the concentration of photoinitiator [474]. These energy values were plotted against $\sqrt{I}$ to form a line of best-fit through the origin. From this linear relationship, the energy required to crosslink GelMA at 4mW/cm2 was 1.26J. By applying $E = tI$, the minimum time thus required to crosslink GelMA at the desired 4mW/cm2 was 314 seconds. To establish a safe margin ensuring the material was fully crosslinked, this timeframe was rounded up to 400 seconds and used for all subsequent UV-curing experiments at 4mW/cm2. E) Temperature analysis of non-crosslinked GelMA from 37oC to 4oC demonstrated a sol-gel transition at 15oC. F) The viscosity was then immediately assessed after cooling to reflect bioprinting conditions. The material exhibited typical shear-thinning properties at 4oC.

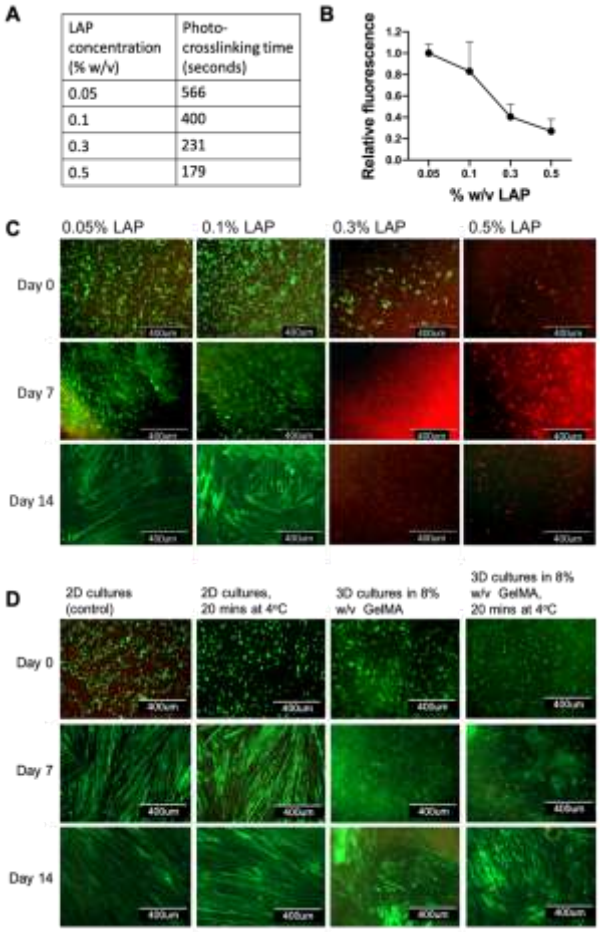

Figure A2. Optimisation of photocuring conditions for myoblast viability in GelMA. A) A range of UV crosslinking times were calculated for different concentrations of lithium phenyl-2,4,6-trimethylbenzoylphosphinate (LAP), based on known kinetic relationships for GelMA between energy, light intensity and crosslinking rate. This was to achieve the same degree of crosslinking between different photocuring configurations. A very low intensity of UV light (4mW/cm2) was chosen to minimise cytotoxicity. B) These conditions were applied to myoblasts encapsulated in 8% w/v GelMA in a series of cytotoxicity screening tests. Metabolic assays (Cell Titre Blue) of cells in proliferation demonstrated a clear threshold of toxicity associated with higher concentrations of LAP. Error bars represent standard deviation. C) Live (green) / dead (red) cell stains over two weeks of differentiation similarly demonstrated high cell viability in cultures with ≤ 0.1% w/v LAP, while cultures with ≥ 0.3% w/v LAP had no viable cells by the end of the study. In addition, the myoblasts in 0.05% and 0.1% LAP were able to mature into myofibres. D) A further cell viability study was conducted with the additional condition of cooling cell cultures to 4oC. Myoblasts grown on tissue culture plastic (2D cultures) and encapsulated in 8% w/v GelMA (3D cultures) were stored at 4oC for 20 minutes. The 3D cultures were then UV-crosslinked, and all cultures were incubated in tissue culture conditions at 37oC and 5% CO2. Subsequent live/dead cell stains showed that cooling to 4oC did not adversely affect cell viability nor the ability for myoblasts to fuse into myofibres.

References

1. Turner NJ, Badylak SF. Regeneration of skeletal muscle. Cell Tissue Res. 2012 Mar 1;347(3):759–74.
2. Grogan BF, Hsu JR, Skeletal Trauma Research Consortium. Volumetric muscle loss. J Am Acad Orthop Surg. 2011;19 Suppl 1:35–7.
3. Nowak KJ, Davies KE. Duchenne muscular dystrophy and dystrophin: pathogenesis and opportunities for treatment. EMBO Rep. 2004 Sep;5(9):872–6.
4. Cittadella Vigodarzere G, Mantero S. Skeletal muscle tissue engineering: strategies for volumetric constructs. Front Physiol. 2014;5(62):362.
5. Ngan CGY, Quigley A, Kapsa RMI, Choong PFM. Engineering skeletal muscle - from two to three dimensions. J Tissue Eng Regen Med. 2017 Jan 8.
6. Jiwlawat S, Lynch E, Glaser J, Smit-Oistad I, Jeffrey J, Van Dyke JM, et al. Differentiation and sarcomere formation in skeletal myocytes directly prepared from human induced pluripotent stem cells using a sphere-based culture. Differentiation. 2017 Aug;96:70–81.
7. Ostrovidov S, Ahadian S, Ramon Azcon J, Hosseini V, Fujie T, Parthiban SP, et al. Three-dimensional co-culture of C2C12/PC12 cells improves skeletal muscle tissue formation and function. J Tissue Eng Regen Med. 2014 Nov 1;:n/a–n/a.
8. Smith AST, Passey S, Greensmith L, Mudera V, Lewis MP. Characterization and optimization of a simple, repeatable system for the long term in vitro culture of aligned myotubes in 3D. J Cell Biochem. Wiley-Blackwell; 2012 Mar;113(3):1044–53.
9. Kang H-W, Lee SJ, Ko IK, Kengla C, Yoo JJ, Atala A. A 3D bioprinting system to produce human-scale tissue constructs with structural integrity. 2016 Feb 15;34(3):312–9.
10. Kim JH, Seol Y-J, Ko IK, Kang H-W, Lee YK, Yoo JJ, et al. 3D Bioprinted Human Skeletal Muscle Constructs for Muscle Function Restoration. Sci Rep. 2018 Aug 17;8(1):12307.
11. Billiet T, Gevaert E, De Schryver T, Cornelissen M, Dubruel P. The 3D printing of gelatin methacrylamide cell-laden tissue-engineered constructs with high cell viability. Biomaterials. 2014 Jan;35(1):49–62.
12. Duchi S, Onofrillo C, O'Connell CD, Blanchard R, Augustine C, Quigley AF, et al. Handheld Co-Axial Bioprinting: Application to in situ surgical cartilage repair. Sci Rep. Nature Publishing Group; 2017 Jul 19;7(1):5837.
13. Liu W, Heinrich MA, Zhou Y, Akpek A, Hu N, Liu X, et al. Extrusion Bioprinting of Shear-Thinning Gelatin Methacryloyl Bioinks. Adv Healthc Mater. 2017 Jun;6(12):1601451.
14. Shi X, Ostrovidov S, Zhao Y, Liang X, Kasuya M, Kurihara K, et al. Microfluidic Spinning of Cell-Responsive Grooved Microfibers. Advanced Functional Materials. 2015 Feb 26;25(15):2250–9.
15. Aubin H, Nichol JW, Hutson CB, Bae H, Sieminski AL, Cropek DM, et al. Directed 3D cell alignment and elongation in microengineered hydrogels. Biomaterials. 2010 Sep;31(27):6941–51.
16. Hosseini V, Ahadian S, Ostrovidov S, Camci-Unal G, Chen S, Kaji H, et al. Engineered Contractile Skeletal Muscle Tissue on a Microgrooved Methacrylated Gelatin Substrate. http://dxdoiorg/101089/tentea20120181. Mary Ann Liebert, Inc. 140 Huguenot Street, 3rd Floor New Rochelle, NY 10801 USA; 2012 Nov 20;18(23-24):2453–65.
17. Ostrovidov S, Shi X, Zhang L, Liang X, Kim SB, Fujie T, et al. Myotube formation on gelatin nanofibers – Multi-walled carbon nanotubes hybrid scaffolds. Biomaterials. 2014 Aug;35(24):6268–77.
17.18. Kang, H.-W.; Lee, S.J.; Ko, I.K.; Kengla, C.; Yoo, J.J.; Atala, A. A 3D Bioprinting System to Produce Human-Scale Tissue Constructs with Structural Integrity. Nat Biotechnol. 2016, 34:312–319
18.19. Ursu DC, Urbanchek MG, Nedic A, Cederna PS, Gillespie RB. In vivo characterization of regenerative peripheral nerve interface function. J Neural Eng. 2016 Feb 9;13(2):026012.
19.20. Mian R, Morrison WA, Hurley JV, Penington AJ, Romeo R, Tanaka Y, et al. Formation of new tissue from an arteriovenous loop in the absence of added extracellular matrix. Tissue Engineering. 2000 Dec;6(6):595–603.
20.21. Boos AM, Loew JS, Weigand A, Deschler G, Klumpp D, Arkudas A, et al. Engineering axially vascularized bone in the sheep arteriovenous-loop model. J Tissue Eng Regen Med. 2012 Mar 22;7(8):654–64.
21.22. Tanaka Y, Tsutsumi A, Crowe DM, Tajima S, Morrison WA. Generation of an autologous tissue (matrix) flap by combining an arteriovenous shunt loop with artificial skin in rats: preliminary report. Br J Plast Surg. 2000 Jan;53(1):51–7.
23. Messina A, Bortolotto SK, Cassell OCS, Kelly J, Abberton KM, Morrison WA. Generation of a vascularized organoid using skeletal muscle as the inductive source. FASEB J. Federation of American Societies for Experimental Biology; 2005 Sep;19(11):1570–2.
22.24. Kim, J.H.; Kim, I.; Seol, Y.-J.; Ko, I.K.; Yoo, J.J.; Atala, A.; Lee, S.J. Neural Cell Integration into 3D Bioprinted Skeletal Muscle Constructs Accelerates Restoration of Muscle Function. Nat Commun. 2020, 11:1025
23.25. O'Connell CD, Di Bella C, Thompson F, Augustine C, Beirne S, Cornock R, et al. Development of the Biopen: a handheld device for surgical printing of adipose stem cells at a chondral wound site. Biofabrication. 2016;8(1):015019.
24.26. Loessner D, Meinert C, Kaemmerer E, Martine LC, Yue K, Levett PA, et al. Functionalization, preparation and use of cell-laden gelatin methacryloyl-based hydrogels as modular tissue culture platforms. Nature Protocols. 2016 Apr;11(4):727–46.
27. Todaro M, Quigley A, Kita M, Chin J, Lowes K, Kornberg AJ, et al. Effective detection of corrected dystrophin loci in mdx mouse myogenic precursors. Hum Mutat. Wiley Subscription Services, Inc., A Wiley Company; 2007 Aug;28(8):816–23.
25.28. Sun, W.; Starly, B.; Daly, A.C.; Burdick, J.A.; Groll, J.; Skeldon, G.; Shu, W.; Sakai, Y.; Shinohara, M.; Nishikawa, M.; et al. The Bioprinting Roadmap. Biofabrication 2020. 12;022002.

Formatted: Font: Not Italic, Complex Script Font: Not Italic

Formatted: Font: Not Italic, Complex Script Font: Not Italic

Formatted: Font: Not Italic, Complex Script Font: Not Italic

Formatted: Font: Not Italic, Complex Script Font: Not Italic

26.29. Schmittgen TD, Livak KJ. Analyzing real-time PCR data by the comparative C-T method. Nature Protocols. 2008;3(6):1101–8.
27.30. Jaimovich E, Reyes R, Liberona JL, Powell JA. IP 3receptors, IP 3transients, and nucleus-associated Ca 2+signals in cultured skeletal muscle. Am J Physiol, Cell Physiol. American Physiological SocietyBethesda, MD; 2000 May;278(5):C998–C1010.
28.31. Stubbs SL, Crook JM, Morrison WA, Newcomb AE. Toward clinical application of stem cells for cardiac regeneration. Heart Lung Circ. 2011 Mar;20(3):173–9.
29.32. Ngan CGY, O'Connell CD, Blanchard R, Boyd-Moss M, Williams RJ, Bourke J, et al. Optimising the biocompatibility of 3D printed photopolymer constructs in vitro and in vivo. Biomed Mater. 2019 Mar 27;14(3):035007.
30.33. Bentzinger CF, Wang YX, Rudnicki MA. Building Muscle: Molecular Regulation of Myogenesis. Cold Spring Harbor Perspectives in Biology. 2012 Feb 1;4(2):a008342–2.
31.34. Schiaffino S, Rossi AC, Smerdu V, Leinwand LA, Reggiani C. Developmental myosins: expression patterns and functional significance. Skelet Muscle. 2015;5(1):22.
32.35. Hernández-Hernández JM, García-González EG, Brun CE, Rudnicki MA. The myogenic regulatory factors, determinants of muscle development, cell identity and regeneration. Seminars in Cell & Developmental Biology. Academic Press; 2017 Dec 1;72:10–8.
33.36. Grifone R, Demignon J, Houbron C, Souil E, Niro C, Seller MJ, et al. Six1 and Six4 homeoproteins are required for Pax3 and Mrf expression during myogenesis in the mouse embryo. Development. 2005 May;132(9):2235–49.
34.37. Capote J, Bolaños P, Schuhmeier RP, Melzer W, Caputo C. Calcium transients in developing mouse skeletal muscle fibres. J Physiol (Lond). 2005 Apr 15;564(Pt 2):451–64.
35.38. Sciancalepore M, Afzalov R, Buzzin V, Jurdana M, Lorenzon P, Ruzzier F. Intrinsic ionic conductances mediate the spontaneous electrical activity of cultured mouse myotubes. Biochim Biophys Acta. 2005 Dec 30;1720(1-2):117–24.
36.39. Cognard C, Constantin B, Rivet-Bastide M, Imbert N, Besse C, Raymond G. Appearance and evolution of calcium currents and contraction during the early post-fusional stages of rat skeletal muscle cells developing in primary culture. Development. The Company of Biologists Ltd; 1993 Mar;117(3):1153–61.
37.40. Wang Y, Ma M, Wang J, Zhang W, Lu W, Gao Y, et al. Development of a Photo-Crosslinking, Biodegradable GelMA/PEGDA Hydrogel for Guided Bone Regeneration Materials. Materials. Multidisciplinary Digital Publishing Institute; 2018 Aug 3;11(8):1345.
38.41. Engler AJ, Griffin MA, Sen S, Bönnemann CG, Sweeney HL, Discher DE. Myotubes differentiate optimally on substrates with tissue-like stiffness. The Journal of Cell Biology. 2004 Sep 13;166(6):877–87.
39.42. Griffin MA, Sen S, Sweeney HL, Discher DE. Adhesion-contractile balance in myocyte differentiation. Journal of Cell Science. 2004 Nov 15;117(Pt 24):5855–63.
40.43. Subramanian A, Krishnan UM, Sethuraman S. Development of biomaterial scaffold for nerve tissue engineering: Biomaterial mediated neural regeneration. Journal of Biomedical Science. BioMed Central; 2009;16(1):108.
41.44. Engler AJ, Sen S, Sweeney HL, Discher DE. Matrix elasticity directs stem cell lineage specification. Cell. 2006 Aug 25;126(4):677–89.
42.45. Aparnathi MK, Patel JS. Biodegradable Gelatin Methacrylate Gel as a Potential Scaffold for Bone Tissue Engineering of Canine Adipose-Derived Stem Cells. J Stem Cells. 2016;11(3):111–9.
43.46. Zhao X, Sun X, Yildirimer L, Lang Q, Lin ZYW, Zheng R, et al. Cell infiltrative hydrogel fibrous scaffolds for accelerated wound healing. Acta Biomaterialia. 2017 Feb;49:66–77.
44.47. O'Connell CD, Zhang B, Onofrillo C, Duchi S, Blanchard R, Quigley A, et al. Tailoring the mechanical properties of gelatin methacryloyl hydrogels through manipulation of the photocrosslinking conditions. Soft Matter. 2018 Mar 14;14(11):2142–51.

Formatted: Normal